Volume 12 | Number 31 | 21 August 2016 | Pages 6499–6676

Soft Matter

www.softmatter.org

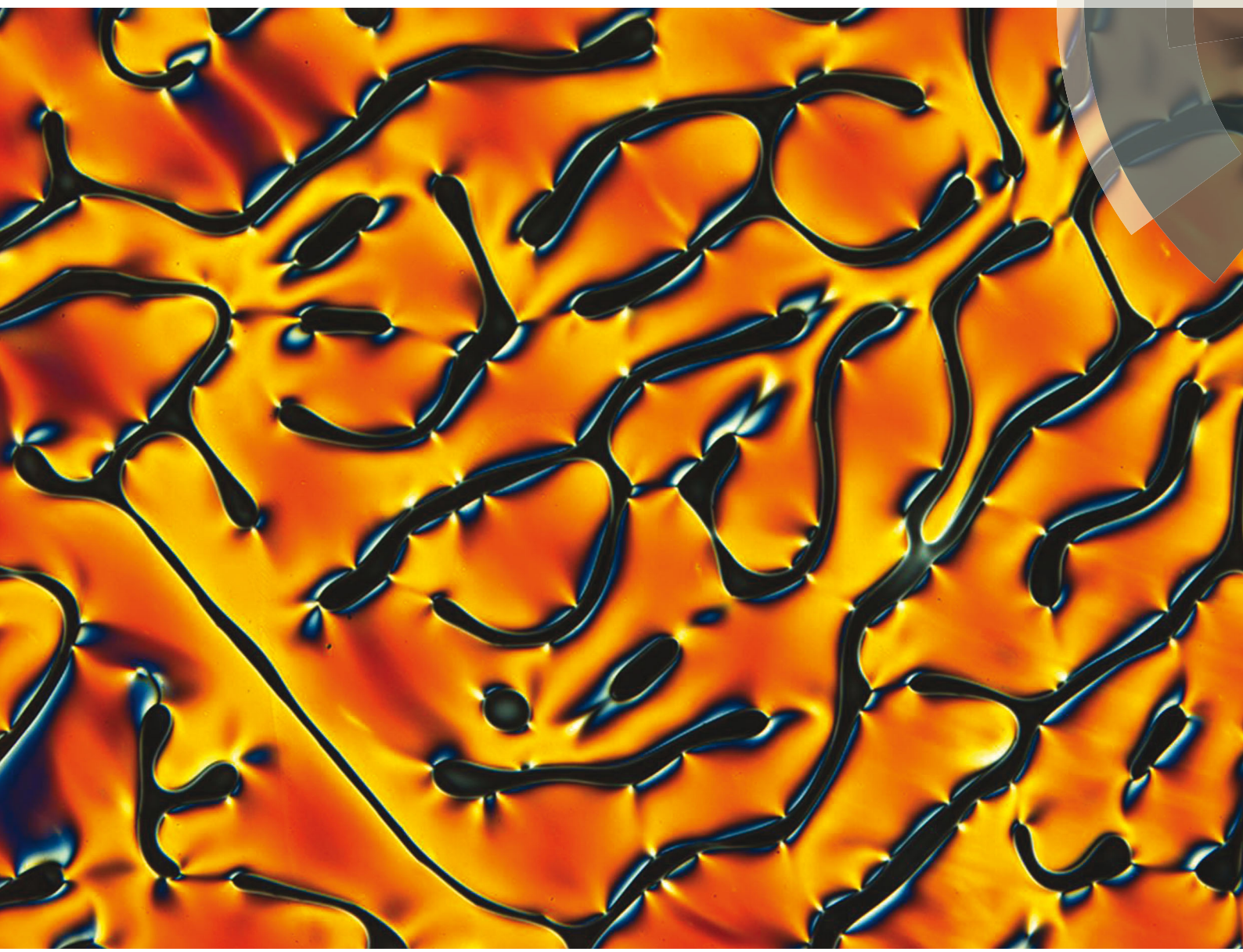

ISSN 1744-683X

ROYAL SOCIETY OF CHEMISTRY

PAPER
Paul H. J. Kouwer *et al.*
Directed peptide amphiphile assembly using aqueous liquid crystal templates in magnetic fields

175 YEARS

Soft Matter

PAPER

View Article Online
View Journal | View Issue

Cite this: *Soft Matter*, 2016, 12, 6518

Directed peptide amphiphile assembly using aqueous liquid crystal templates in magnetic fields†

Pim van der Asdonk,‡[ab] Masoumeh Keshavarz,‡[abc] Peter C. M. Christianen[bc] and Paul H. J. Kouwer*[ab]

Received 16th March 2016,
Accepted 12th June 2016

DOI: 10.1039/c6sm00652c

www.rsc.org/softmatter

An alignment technique based on the combination of magnetic fields and a liquid crystal (LC) template uses the advantages of both approaches: the magnetic fields offer non-contact methods that apply to all sample sizes and shapes, whilst the LC templates offer high susceptibilities. The combination introduces a route to control the spatial organization of materials with low intrinsic susceptibilities. We demonstrate that we can unidirectionally align one such material, peptide amphiphiles in water, on a centimeter scale at a tenfold lower magnetic field by using a lyotropic chromonic liquid crystal as a template. We can transform the aligned supramolecular assemblies into optically active π-conjugated polymers after photopolymerization. Lastly, by reducing the magnetic field strength needed for addressing these assemblies, we are able to create more complex structures by initiating self-assembly of our supramolecular materials under competing alignment forces between the magnetically induced alignment of the assemblies (with a positive diamagnetic anisotropy) and the elastic force dominated alignment of the template (with a negative diamagnetic anisotropy), which is directed orthogonally. Although the approach is still in its infancy and many critical parameters need optimization, we believe that it is a very promising technique to create tailor-made complex structures of (aqueous) functional soft matter.

Introduction

Self-assembly in aqueous solutions is an excellent approach to fabricate functional materials that can interface with biological and biochemical processes, for instance within sensing devices.[1–3] Controlling the macroscopic organization (such as micropatterns and alignment) of such aqueous supramolecular materials across multiple length scales is essential for device performance,[4–7] but remains a major challenge to date. Over the years, many techniques have been developed to control the spatial organization of aqueous self-assembling materials, including photolithography,[8,9] soft lithography,[9,10] electrospinning,[11–13] electric fields[14–17] and magnetic fields.[18–20] All these techniques have demonstrated their use in specific situations, but they also suffer from limitations that are often directly associated to the organization of aqueous soft materials. For instance, such materials frequently display a low susceptibility and incompatibility to strong electric fields. Also complex pattern formation of these structures over multiple length scales on a wide range of surfaces is very challenging.

We recently explored liquid crystal templating as a tool to direct the spatial organization of supramolecular materials in water.[21] This approach offers a number of unique advantages: (i) LC templating does not depend on delicate molecular interactions and is therefore suitable to organize a wide range of soft materials; (ii) the liquid crystal (LC) template itself is highly susceptible to external stimuli and is readily manipulated to generate complex patterns; (iii) after alignment, organization and optional post-modification, the LC template can be removed, leaving only the aligned functional material on the substrate. LC templating has been applied successfully to align organic[22–31] and, to a lesser extent, aqueous functional materials[32–37] Mostly, surface interactions were used to control the alignment of aqueous soft matter, although one example of carbon nanotube alignment in a magnetic field aligned lyotropic liquid crystal was published.[32]

Here, we use the advantages of LC templating and combine them with the unique features of magnetic field alignment, which is an intrinsic contact-free alignment technique (no specific directing surfaces needed). We demonstrate that this approach allows for the formation of complex patterns by cleverly exploiting

[a] Department of Molecular Materials, Radboud University, Heyendaalseweg 135, 6525 AJ Nijmegen, The Netherlands. E-mail: p.kouwer@science.ru.nl
[b] Institute for Molecules and Materials, Radboud University, Heyendaalseweg 135, 6525 AJ Nijmegen, The Netherlands
[c] High Field Magnet Laboratory (HFML - EMFL), Radboud University, Toernooiveld 7, 6525 ED Nijmegen, The Netherlands

† Electronic supplementary information (ESI) available. See DOI: 10.1039/c6sm00652c

‡ These authors contributed equally.

the differences in sign and strength of the diamagnetic anisotropies of the LC template and the dispersed soft material.

To demonstrate this concept, we aligned and patterned peptide amphiphiles (**PA**) in a lyotropic chromonic liquid crystal (LCLC) template in a magnetic field. In an aqueous LCLC template solution, **PA** self-assembles into nanometer-wide fibers and progressively bundles into hierarchical micron to millimeter-sized structures. We show that we need a tenfold lower magnetic field to align these amphiphilic bundles over a centimeter range in the presence of the magnetically responsive LCLC template. Post-modification provides an easy method to introduce functionality and dimensional stability to the structures; the latter allows for removal of the template by washing. The reduction of the magnetic field alignment threshold opens up a window for the creation of more complex structures at high magnetic fields. Here, we anticipate a competition between the magnetically induced alignment of the **PA** assemblies (with a positive diamagnetic anisotropy) and the elastic force dominated alignment of the template (with a negative diamagnetic anisotropy), which is directed orthogonally.

Materials and methods

The peptide amphiphile that we use are self-assembling supramolecular materials which have shown a lot of promise in both biomedical engineering and sensing applications.[38–45] Its synthesis and characterization has been reported before.[21,45] The amphiphile consists of a 25 carbon hydrophobic tail and a GAGAK hydrophilic head section (Fig. 1a). In both water and in nematic **DSCG** at room temperature, **PA** self-assembles due to hydrophobic–hydrophilic interactions, forming long 1D beta-sheet fibers (Fig. 1b). In water, these beta-sheets form isotropic assemblies at larger length scales.[21] Furthermore, **PA** was functionalized with a diacetylene-moiety, which allows us to crosslink these materials by a topological photopolymerization step, resulting in a greatly improved mechanical stability and a strong chromatic response due to the π-conjugated backbones. For device applications, such as in tissue engineering[38,39,41,42] and molecular electro-optics[40] controlled long range ordering of these materials is essential. Macroscopic alignment was realized with shear flow,[38,40,46] electrospinning[13] and a high magnetic field approach,[18,19] whereas multi-length scale control was accomplished using soft lithography[47] and recently with an LCLC template on photopatterned substrates.[21] The high magnetic field experiments showed that, at sufficient field strengths, **PA** assemblies align with their long axis parallel to the magnetic fields (with the hydrogen bonds parallel and the alkyl chains perpendicular to the field).[18,48] The magnetic alignment of such materials depends on the anisotropy of the diamagnetic susceptibility and the strength of the applied field. We calculated a value of $\Delta\chi = \Delta\chi_{\parallel} - \Delta\chi_{\perp} \approx -611 \times 10^{-12}$ m^3 mol^{-1} for the molar diamagnetic susceptibility for **PA** (see ESI†). The number is negative (*i.e.* **PA** will align with the molecular axis perpendicular to the field, but 1D assemblies will align parallel to the field) and small, which confirms that even for large assemblies high magnetic fields are necessary to obtain alignment.

We chose disodium cromoglycate (**DSCG**) as a lyotropic chromonic liquid crystal (LCLC) template to direct the organization of **PA** in magnetic fields. **DSCG** is a rigid plank-like molecule that consists of an aromatic core with water-solubilizing groups on the periphery (Fig. 1a). In water, the molecules stack face-to-face in columnar aggregates due to π–π stacking and hydrophobic interactions, and at certain concentrations and temperatures, these aggregates form nematic and smectic phases.[49] Recently, nematic **DSCG** solutions have been used to template the organization of motile bacteria[35–37] and the alignment of carbon nanotubes[34] and peptide amphiphiles.[21]

The molar diamagnetic susceptibility of **DSCG** is positive and much larger. We calculated a value of $\Delta\chi = \chi_{\parallel} - \chi_{\perp} \approx 1226 \times 10^{-12}$ m^3 mol^{-1}. Now the molecules will order with their long axis parallel to the field and the 1D assemblies will order in a plane perpendicular to it. As the concentration **DSCG** is much higher than the concentration **PA**, one expects that **DSCG** can be aligned at much lower field strengths. Indeed, experimentally was found that magnetic fields as low as 0.7 T[50,51] are sufficient to align a nematic solution of **DSCG**. By placing **DSCG** solutions in a confined space (such as in a glass cell of a several microns spacing), the stacks are forced to align in-plane and perpendicular to the magnetic field vector. The ability of **DSCG**

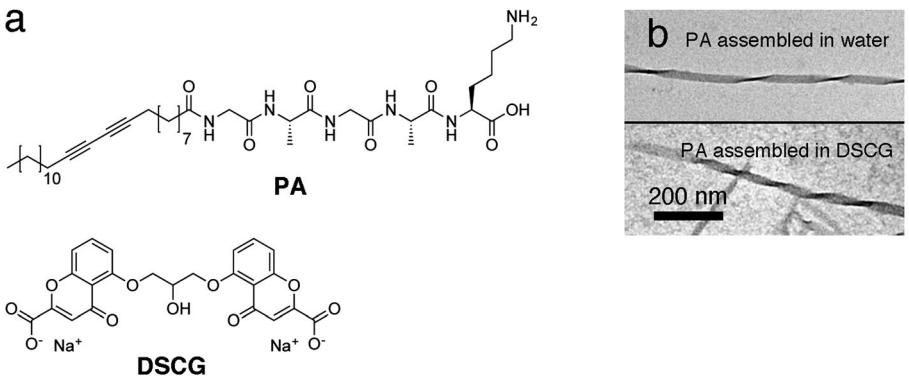

Fig. 1 Molecular structures (a) of **PA** and **DSCG**. Transmission electron microscopy (b) images of **PA** assembled in water (top) and in nematic **DSCG** in water (bottom), showing in both cases a fibrous twisted beta-sheet structure.

to act as an aqueous anisotropic solvent which can direct other dispersed materials, while also having relatively high magnetic susceptibilities, makes this particular template an excellent material to control the structural organization of **PA**s, but potentially a much wider range of aqueous functional soft materials using magnetic fields.

Results and discussion

Unidirectional aligned arrays of π-conjugated peptide amphiphiles

To create unidirectionally aligned arrays of dichromic **PA**s, we filled glass cells (23 micron spacing) with a mixture of **PA** (0.026 wt%) and **DSCG** (13.7 wt%) in milli-Q. The glass cells were sealed with epoxy glue to prevent water evaporation and after 1 hour of drying, the cells were loaded in the magnetic field setup. The temperature was increased to 80 °C after which a magnetic field (**B** = 2 T) was turned on. With the magnetic field on, the sample was cooled to room temperature over a period of 40–60 minutes. Subsequently, the magnet field was switched off and the sample was removed. Polarized optical microscopy (POM) was used to investigate the assembly and alignment of **PA** and **DSCG**.

Fig. 2 shows microscopy images of **PA** and **DSCG** after cooling to room temperature in the presence of a 2 T magnetic field. **DSCG** forms a unidirectionally aligned monodomain over centimeter dimensions (Fig. 2a). The **DSCG** stacks are aligned in-plane and perpendicular to the direction of the magnetic field, as confirmed by analyzing the optical appearance after inserting a quarter wave plate between analyzer and sample in the POM stage (Fig. S1, ESI†). Over the same centimeter length scales, OM reveals extended fibrous bundles aligned (Fig. 2b), which are macroscopically aligned self-assembled **PA** fibers, oriented parallel to the **DSCG** template and thus perpendicular to the magnetic field direction. Furthermore, in many locations, spindle-like structures are observed (Fig. 2c) from which aligned fibrous bundles emerge. We believe that these spindles are nucleation sites of the initial **PA** fibers formation from which (aligned) fiber growth was initiated later in the cooling process.

After assembly in the magnetic field, a photopolymerization step (initiated by leaving the glass cells uncovered on a lab table for several hours or by a 10 minute illumination with a conventional UV-lamp) crosslinked the aligned **PA** bundles, which consequently became bright blue in color due to the π-conjugated backbone structure (Fig. 2b and c). At this stage, the cells were opened and **DSCG** was washed away, leaving mechanically stable **PA** bundles (as a result of the photopolymerization process) organized unidirectionally on the substrate. Scanning electron microscopy (SEM, Fig. 2d) shows massive arrays of fibrous **PA** bundles unidirectionally aligned perpendicular to the magnetic field. Control experiments demonstrated the role of the liquid crystalline template. Without **DSCG** present, we found no macroscopic fiber alignment for either the samples grown in the absence (Fig. S2, ESI†) or in the presence (Fig. S3, ESI†) of the magnetic field.

Mixtures of **PA** in **DSCG** in the absence of a magnetic field showed random in-plane LCLC alignment, resulting the formation of disordered fibers (Fig. S4, ESI†). We found that the applied

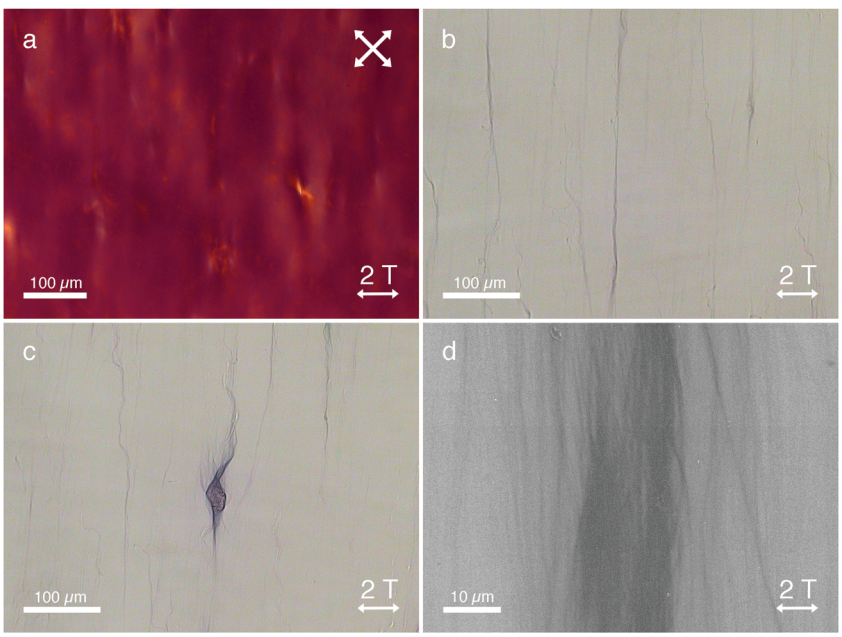

Fig. 2 Microscopy images of **PA** (0.026 wt%) in a nematic **DSCG** template (13.7 wt% in milli-Q) after alignment in a 2 T magnetic field. POM image (a) shows a unidirectionally aligned monodomain of **DSCG**. OM image (b) shows photopolymerized **PA** bundles aligned along the direction of **DSCG** template. Image (c) shows an example of the spindle-like structures also present in the **DSCG** template. After opening the cell and washing away **DSCG**, scanning electron microscopy (SEM) image (d) shows an aligned photopolymerized **PA** bundle in greater detail. White double-sided arrows indicate the direction of the applied magnet field.

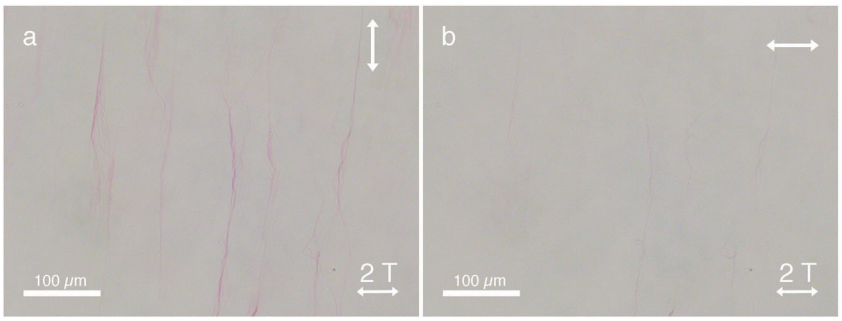

Fig. 3 Microscopy images of **PA** (0.026 wt%) in **DSCG** (13.7 wt% in milli-Q) after alignment in a 2 T magnetic field, showing a strong dichroic response. The temperature of the sample was raised to 65 °C (isotropic phase of **DSCG**) to remove dichroic contribution from the **DSCG** birefringence. The double-sided white arrows in the top right corner indicate the orientation of the polarizer in the OM stage. When the polarizer is aligned along the backbone of the **PA** assemblies (a) light is strongly absorbed due to the aligned π-conjugated backbones. When the polarizer is oriented perpendicular to the backbones of the **PA**, light absorption is reduced (b). Due to the increased temperature, the **PA** bundles undergo a color change from blue to red.

magnetic field has no observable influence on the observed **PA** bundle morphology; the microscopy images of mixtures of **PA** and **DSCG** assembled in the absence of a magnetic field (Fig. S5, ESI†) show similar **PA** assembly morphologies, compared to when **PA** is assembled in a **DSCG** template with a magnetic field applied (Fig. 2).

Due to the macroscopic unidirectional alignment of the π-conjugated backbones of these amphiphilic polydiacetylenes, strong linear dichroism is induced (Fig. 3). Linearly polarized light parallel to the backbone of the **PA** assemblies is strongly absorbed (Fig. 3a), whereas the absorption of linearly polarized light oriented perpendicular to the assemblies is drastically reduced (Fig. 3b). Additionally, the polymerized assemblies are very stable in demanding conditions (Fig. S6, ESI†), even at temperatures as high as 90 °C.[21]

Fig. 4 schematically displays the templating mechanism responsible for macroscopic **PA** alignment. At high temperatures (> 80 °C) both **PA** (grey, Fig. S7, ESI†) and **DSCG**[49] (yellow) are (mostly) molecularly dissolved (Fig. 4a). Cooling to 50 °C initiates self-assembly of **PA** fibers, which are not responsive to the 2 T magnetic field thus orient isotropically (Fig. 4b). Simultaneously during cooling, the self-assembled **DSCG** stacks have grown long enough to form nematic LCLC domains wherein the stacks align perpendicular to the magnetic field

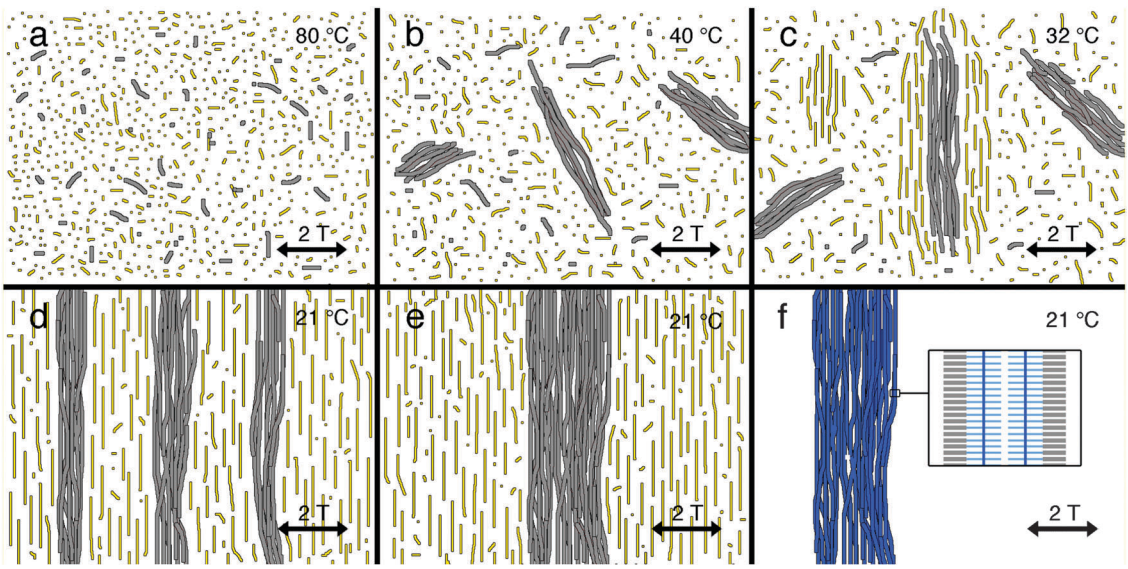

Fig. 4 Cartoon of the mechanism of LCLC (yellow) templated **PA** (grey) alignment in low (2 T) magnetic fields. Cooling the sample from a molecularly dissolved **PA** and **DSCG** solution at high temperatures (panel a) first leads to **PA** assembly which are not affected by the small magnetic field (panel b). At slightly lower temperatures, we find the **DSCG** transition into the nematic–isotropic biphasic regime. The nematic droplet (in an isotropic coninuum) are aligned by the 2 T field and the **PA** in them will be reoriented by the liquid crystalline matrix (panel c). Further cooling increases the fraction of (aligned) nematic **DSCG** solution until at room temperature a continuous nematic phase is formed. At the same time, the **PA** monomers continue to assemble into increasingly long fibers. As their environment now is homogeneously aligned (panel d), we find full efficient templating to the **PA** assemblies. Keeping the sample at room temperature results in a further (lateral) assembly process of the **PA** fibers (panel e). At this stage, the fibers can be photopolymerized (blue colored fibers) and the template can be removed (panel f). The inset in panel f shows the position of the individual **PA** monomers with respect to the bundle's long axis. The dark blue vertical bar indicates direction of the π-conjugated backbone after photopolymerization.

(Fig. 4c) as a result of their negative diamagnetic anisotropy. The presence of **PA** bundles may facilitate LCLC formation (Fig. S8, ESI†) since we observed a slight increase (from 32.7 to 33.7 °C) in the clearing temperature of **DSCG** (13.4 wt%) with **PA** present. Whilst the LC domains expand into a single monodomain, reorienting shear forces and elastic mediated forces direct the alignment of **PA** nanofibers parallel to the LCLC template (Fig. 4d). Meanwhile during the cooling process, depletion interactions with the LCLC solvent forces these nanometer-wide fibers to form much thicker bundles (Fig. 4e and Fig. S9, ESI†). After photopolymerization, the **PA** assemblies are very stable due to the crosslinked diacetylene cores which are oriented parallel to the fiber's long axis (indicated by the vertical dark blue line in the inset in Fig. 4f). Due to the increased stability, the template can be readily removed. In addition, the **PA** bundles show strong linear polarized absorption characteristics because of the presence of a transition dipole moment parallel to the π-conjugated polydiacetylene **PA** backbones.

Hierarchically patterned π-conjugated peptide amphiphiles

Besides utilizing a template to realize macroscopic unidirectional peptide amphiphile orientation, we used the orthogonal diamagnetic anisotropies of **DSCG** and **PA** to create complex hierarchical **PA** structures in high magnetic fields. At these high fields, we anticipated a competition between the two **PA** alignment forces: the LCLC templates that directs the orientation perpendicular to the magnetic field and the (high) magnetic field itself, which forces the **PA** stacks to organize parallel to the field.

Sealed glass cells containing **PA** (0.026 wt%) and **DSCG** (13.7 wt% in milli-Q) were placed in a high magnetic field setup. The glass cells were heated to 80 °C and a 20 T magnetic field was applied. After cooling the cells to room temperature, the magnetic field was switched off and the sample was studied with (polarized) optical microscopy (Fig. 5).

Surprisingly, we observed complex LC director fields (Fig. 5a) as well as areas of large single domains in the range of several millimeters (Fig. 5b). In contrast, when **DSCG** was aligned in the absence of **PA** (Fig. S10, ESI†) in a high magnetic field, a perfectly aligned monodomain was obtained. Upon closer inspection with optical microscopy (Fig. 5c), we observed two distinct organizations of fibrous aggregates present everywhere in the sample: (i) fibers aligned parallel to the direction of the applied magnetic field, sometimes in conjunction with spindle-like structures (aligned perpendicular to the field); and (ii) fibers aligned perpendicular to the field in both bundle- and spindle-like formations, identical to the assemblies found after applying a 2 T magnetic field sweep (Fig. 2).

After a photopolymerization step, the orthogonally aligned **PA** assemblies turned blue in color (Fig. 5c), analogous to the assemblies in Fig. 2. After the cross-linking step, the glass cells were opened and the LCLC was washed away. We used SEM (Fig. 6) to investigate the hierarchical structures with the two distinct organizations at higher magnifications in order to unravel its morphology. Fig. 6a–c shows aligned fibrous bundles oriented parallel to the field, in conjunction with perpendicularly aligned spindle-like aggregates. In some locations (Fig. 6d), only spindle-like aggregates were found (oriented perpendicular to the magnetic field) without any conjoined bundles that were aligned parallel to the field. These structures are also visible with optical microscopy (Fig. 5c, top right corner) and are identical to the assemblies found after a 2 T magnetic field sweep (Fig. 2).

We postulate that these two distinct **PA** fiber orientations actually are the result of competition in alignment introduced by the positive diamagnetic susceptibility of **PA** and perpendicular alignment along the LCLC template induced by its negative diamagnetic susceptibility.[52]

Fig. 7 schematically shows the prime processes when cooling the solution from the molecularly dissolved state at 80 °C (Fig. 7a) in the presence of a high (20 T) magnetic field. Again at approximately 50 °C, **PA** fiber (grey) formation commences which now is directed by the strong magnetic field (Fig. 7b), yielding bundles parallel to the field. Due to the time and temperature-dependent depletion interactions and the ongoing **PA** assembly, these fibers continue to grow in dimensions (Fig. 7c). Simultaneously during cooling, small nematic **DSCG** domains form and grow to eventually form large nematic domains throughout the sample. Newly formed and still dissolved **PA** fibers may now follow the elastic forces induced by the nematic **DSCG** phase and orient perpendicular to the fibers that are already present before. They may give rise to new bundles that are entirely aligned perpendicular to the field (Fig. 6d) or associate tangentially to the existing parallel bundles (Fig. 6a–c and 7d).

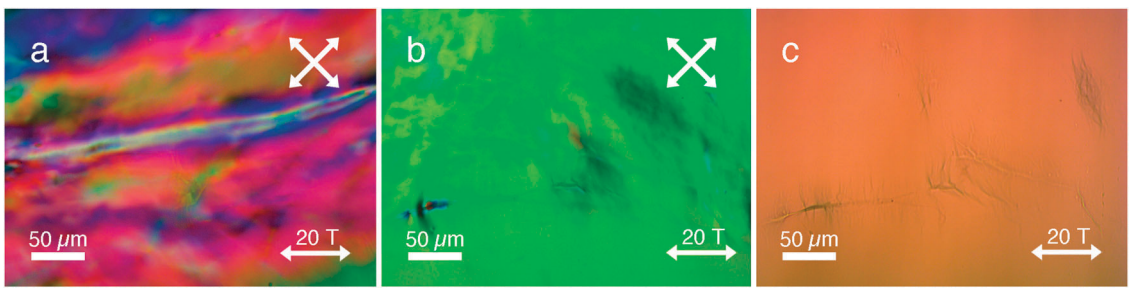

Fig. 5 Microscopy images of **PA** (0.026 wt%) in a nematic **DSCG** template (13.7 wt% in milli-Q) after 20 T magnetic field alignment. POM image (a) shows complex in-plane nematic LCLC director orientations. POM image (b) shows large single LCLC domain, where (after removal of polarizers from POM stage) aligned **PA** aggregates are visible aligned both perpendicular and parallel to the magnetic field (c).

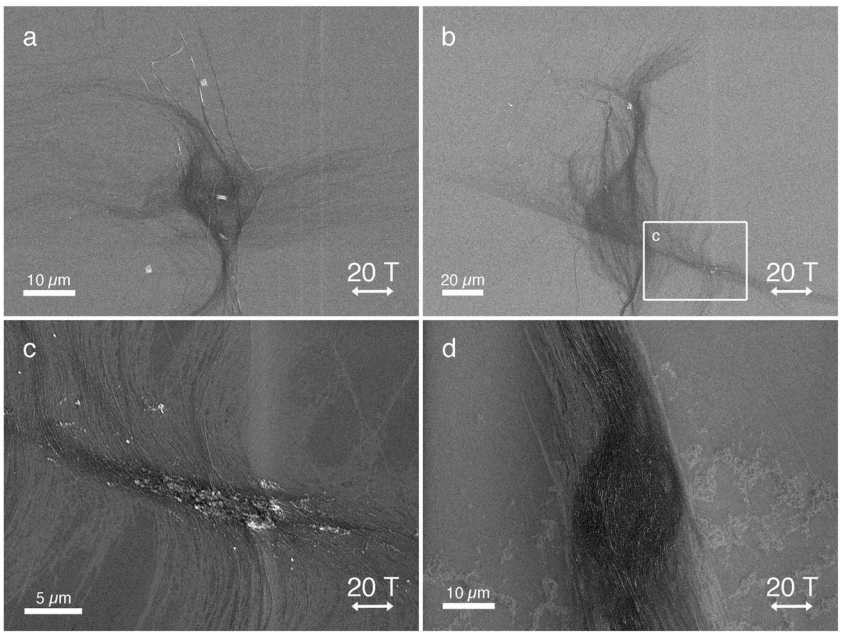

Fig. 6 SEM images of **PA** (0.026 wt%) in a nematic **DSCG** template (13.7 wt% in milli-Q) after alignment in a 20 T magnetic field. SEM Images (a and b) show orthogonally aligned **PA** assemblies with fibers oriented both perpendicular and parallel to the magnetic field. Image (c) shows unraveled fibers (perpendicular aligned to the field) from the thicker unidirectionally aligned bundle (parallel to the field). Image (d) shows a unidirectionally aligned spindle similar to a 2 T aligned **PA** bundle (Fig. 2c).

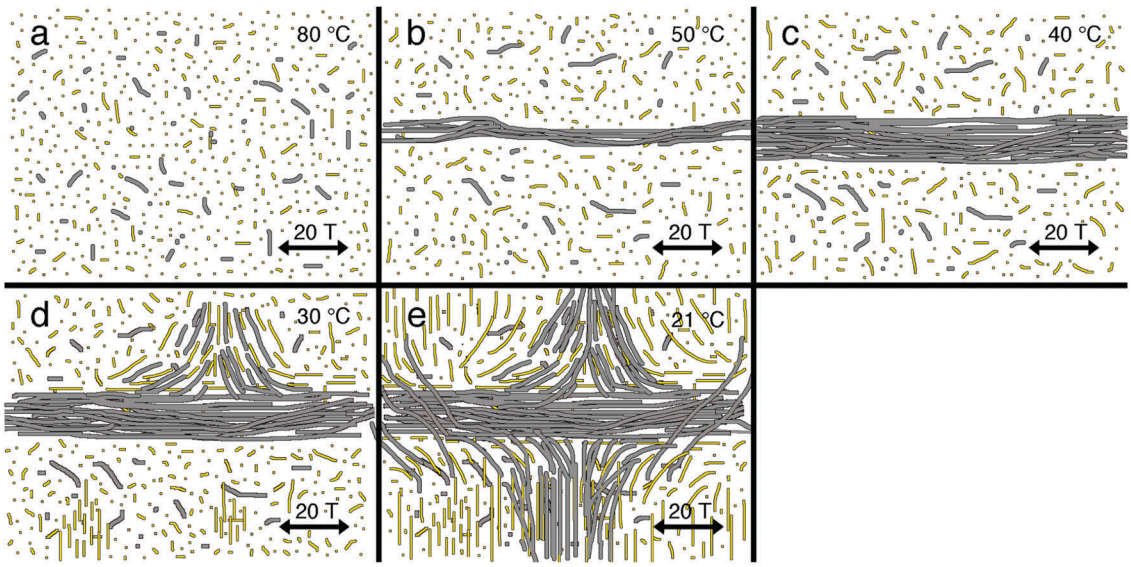

Fig. 7 Cartoon of the mechanism of LCLC (yellow) templated **PA** (grey) alignment in high (20 T) magnetic fields, again starting from a high temperature solution with **DSCG** and **PA** molecularly dissolved (panel a). Upon cooling the sample, **PA** fibers start forming first. In the 20 T magnetic field, these fibers start growing parallel to the field (the monomers with negative $\Delta\chi$ perpendicular to the field) and expanding (panels b and c). At the clearing temperature of the **DSCG** solution, nematic droplets form, in which the **DSCG** aggregates are oriented perpendicular to the field. These droplets and, at lower temperatures, the homogeneously aligned **DSCG** solution will then template further **PA** fiber growth in the direction of the nematic matrix and thus perpendicular to early formed fibers (panels d and e).

The elastic forces are not high enough to reorient large **PA** bundles, which maintain their parallel orientation. One should consider, however, that phase formation in **DSCG** sets in at a lower temperature than **PA** assembly. The fact that we see significant amounts of perpendicularly oriented **PA** fibers suggests that the elastic forces are stronger than the magnetic forces (at 20 T). This is supported by the observation of tiny fibers emerging from the large parallel aligned bundles that unravel and predominantly bend in the direction of the nematic LCLC template (Fig. 6c). These assemblies then act as a

nucleation point for further **PA** assembly and bundling until room temperature is reached (Fig. 7e).

When conducting the same experiment at a lower magnetic field of 15 T, **PA** neither formed assemblies that aligned parallel to the field nor orthogonal bundled aggregates. Instead, only homogeneously aligned structures as in Fig. 2 and Fig. 6d (perpendicular to the magnetic field direction and parallel to the **DSCG** stacks) were observed (Fig. S11a and b, ESI†). We found similar **PA** aggregates (again perpendicular to the field) when **PA** was assembled at lower concentrations (0.013 wt%) in a **DSCG** template at 20 T (Fig. S11c, ESI†). Apparently, at these lower concentrations the assembly of **PA** is dominated by the LCLC template despite the presence of the high magnetic field. On the other hand, at increased **PA** concentrations (0.039 wt%), the orthogonal structures similar to the ones in Fig. 5c and 6a, b were observed (Fig. S11d, ESI†). The higher **PA** concentrations result in the formation of larger assemblies which in turn have an increased diamagnetic susceptibility and hence an increased responsiveness to the magnetic field.[48] This is further supported by control experiments which show that 0.1 wt% **PA** (without **DSCG** present) assembled at 20 T form macroscopic aligned bundles along the magnetic field direction, while at 0.015 wt% **PA** (without **DSCG** present) at 20 T no macroscopic alignment is observed (Fig. S12, ESI†).

Overall, the structure formation of these supramolecular materials in LCLC templates and magnetic fields depends on the relative strengths of the two opposing contributions, which both can be tuned independently. The shear and elastic forces of the template can be tailored by the particular LCLC used, as well as the temperature and concentration of the template. The diamagnetic susceptibility of **PA** can be tuned by its concentration and also the temperature. In addition, the magnetic field itself is an important parameter as is the (temperature, time and concentration dependent) depletion effect. A more detailed understanding of all of these factors will be the starting point to control and utilize the complex structures that are available through these methods.

Conclusion

In this work, we show that we can create unidirectional aligned arrays of functional supramolecular materials on a centimeter scale by combining LCLC templates with 2 T magnetic fields. After photopolymerization, these materials show strong linear polarized absorption characteristics due to the macroscopic aligned π-conjugated backbones. Their increased mechanical strength also allows for the removal of the LCLC template by a simple washing step, leaving the optically active amphiphiles unidirectionally aligned on the substrate. With this approach it is possible to align these materials at 10 times lower magnetic field strengths than previously reported.[18]

This approach has the great advantage that it can be applied to macroscopically align a wide range of soft matter, since the alignment procedure solely relies on orientational shear and elastic forces and lacks the requirement for delicate molecular interactions that require fine tuning. Since we are also able to drastically lower the requirements for magnetic field alignment with this approach, we envisage the use of small commercially available permanent magnets, for instance based on neodymium, integrated within tabletop setups for applying this technique to a huge number of aqueous functional soft materials.

Additionally, the reduction of the field required for alignment opens up the opportunity to create more complex structures at much higher fields. We created orthogonally aligned **PA** assemblies by exploiting the opposite diamagnetic anisotropies of our LC template and self-assembled amphiphilic materials. Such self-assembled off-equilibrium structures are impossible to create on such a small length scales using other conventional alignment techniques. We believe, therefore, that this approach is very promising to create tailor-made complex structures of (aqueous) functional soft matter highly beneficial for device applications in many diverse areas. A better control of the critical parameters that we set out in the manuscript will be necessary to achieve this.

Acknowledgements

We would like to thank both Britta Ramakers and Dennis Löwik for the synthesis of **PA** and the TechnoCentrum for the fabrication of the cell construction apparatus. This work is supported by NanoNextNL (PvdA, PHJK, grant 07A.07 & MK, grant 07A.06), a micro and nanotechnology consortium of the Government of the Netherlands and 130 partners. Part of this work is supported by EuroMagNET II under the EU Contract No. 228043. We acknowledge the support of the HFML-RU/FOM, member of the European Magnetic Field Laboratory (EMFL).

References

1 M. Gerard, A. Chaubey and B. D. Malhotra, *Biosens. Bioelectron.*, 2002, **17**, 345–359.
2 N. K. Guimard, N. Gomez and C. E. Schmidt, *Prog. Polym. Sci.*, 2007, **32**, 876–921.
3 S. Cosnier and M. Holzinger, *Chem. Soc. Rev.*, 2011, **40**, 2146–2156.
4 F. J. M. Hoeben, P. Jonkheijm, E. W. Meijer and A. P. H. J. Schenning, *Chem. Rev.*, 2005, **105**, 1491–1546.
5 L. C. Palmer and S. I. Stupp, *Acc. Chem. Res.*, 2008, **41**, 1674–1684.
6 T. Aida, E. W. Meijer and S. I. Stupp, *Science*, 2012, **335**, 813–817.
7 B. Su, Y. Wu and L. Jiang, *Chem. Soc. Rev.*, 2012, **41**, 7832–7856.
8 Z. Nie and E. Kumacheva, *Nat. Mater.*, 2008, **7**, 277–290.
9 H. M. Saavedra, T. J. Mullen, P. Zhang, D. C. Dewey, S. A. Claridge and P. S. Weiss, *Rep. Prog. Phys.*, 2010, **73**, 036501.
10 B. D. Gates, Q. Xu, M. Stewart, D. Ryan, C. G. Willson and G. M. Whitesides, *Chem. Rev.*, 2005, **105**, 1171–1196.
11 D. Li, Y. Wang and Y. Xia, *Adv. Mater.*, 2004, **16**, 361–366.
12 D. Yang, B. Lu, Y. Zhao and X. Jiang, *Adv. Mater.*, 2007, **19**, 3702–3706.

13 A. S. Tayi, E. T. Pashuck, C. J. Newcomb, M. T. McClendon and S. I. Stupp, *Biomacromolecules*, 2014, **15**, 1323–1327.
14 M. Wang, L. Du, X. Wu, S. Xiong and P. K. Chu, *ACS Nano*, 2011, **5**, 4448–4454.
15 L. Sardone, V. Palermo, E. Devaux, D. Credgington, M. de Loos, G. Marletta, F. Cacialli, J. van Esch and P. Samorì, *Adv. Mater.*, 2006, **18**, 1276–1280.
16 Y. Shoji, M. Yoshio, T. Yasuda, M. Funahashi and T. Kato, *J. Mater. Chem.*, 2009, **20**, 173–179.
17 M. Yoshio, Y. Shoji, Y. Tochigi, Y. Nishikawa and T. Kato, *J. Am. Chem. Soc.*, 2009, **131**, 6763–6767.
18 D. W. P. M. Löwik, I. O. Shklyarevskiy, L. Ruizendaal, P. C. M. Christianen, J. C. Maan and J. C. M. van Hest, *Adv. Mater.*, 2007, **19**, 1191–1195.
19 M. van den Heuvel, A. M. Prenen, J. C. Gielen, P. C. M. Christianen, D. J. Broer, D. W. P. M. Löwik and J. C. M. van Hest, *J. Am. Chem. Soc.*, 2009, **131**, 15014–15017.
20 M. Wallace, A. Z. Cardoso, W. J. Frith, J. A. Iggo and D. J. Adams, *Chem. – Eur. J.*, 2014, **20**, 16484–16487.
21 P. van der Asdonk, H. C. Hendrikse, M. F.-C. Romera, D. Voerman, B. E. I. Ramakers, D. W. P. M. Löwik, R. P. Sijbesma and P. H. J. Kouwer, *Adv. Funct. Mater.*, 2016, **26**, 2609–2616.
22 T. Kato, Y. Hirai, S. Nakaso and M. Moriyama, *Chem. Soc. Rev.*, 2007, **36**, 1857–2128.
23 Y. Hirai, S. S. Babu, V. K. Praveen, T. Yasuda, A. Ajayaghosh and T. Kato, *Adv. Mater.*, 2009, **21**, 4029–4033.
24 K. Akagi, G. Piao, S. Kaneko, K. Sakamaki, H. Shirakawa and M. Kyotani, *Science*, 1998, **282**, 1683–1686.
25 M. Goh, S. Matsushita and K. Akagi, *Chem. Soc. Rev.*, 2010, **39**, 2466–2476.
26 M. D. Lynch and D. L. Patrick, *Nano Lett.*, 2002, **2**, 1197–1201.
27 I. Dierking, G. Scalia, P. Morales and D. LeClere, *Adv. Mater.*, 2004, **16**, 865–869.
28 O. Catanescu and L.-C. Chien, *Adv. Mater.*, 2005, **17**, 305–309.
29 S. Moynihan, P. Lovera, D. O'Carroll, D. Iacopino and G. Redmond, *Adv. Mater.*, 2008, **20**, 2497–2502.
30 X. Tong, D. Han, D. Fortin and Y. Zhao, *Adv. Funct. Mater.*, 2012, **23**, 204–208.
31 J.-W. Chen, C.-C. Huang and C.-Y. Chao, *ACS Appl. Mater. Interfaces*, 2014, **6**, 6757–6764.
32 J. Lagerwall, G. Scalia, M. Haluska, U. Dettlaff-Weglikowska, S. Roth and F. Giesselmann, *Adv. Mater.*, 2007, **19**, 359–364.
33 M. Hara, S. Nagano, N. Kawatsuki and T. Seki, *J. Mater. Chem.*, 2008, **18**, 3259.
34 N. Ould-Moussa, C. Blanc, C. Zamora-Ledezma, O. D. Lavrentovich, I. I. Smalyukh, M. F. Islam, A. G. Yodh, M. Maugey, P. Poulin, E. Anglaret and M. Nobili, *Liq. Cryst.*, 2013, **40**, 1628–1635.
35 P. C. Mushenheim, R. R. Trivedi, H. H. Tuson, D. B. Weibel and N. L. Abbott, *Soft Matter*, 2013, **10**, 88.
36 S. Zhou, A. Sokolov, O. D. Lavrentovich and I. S. Aranson, *Proc. Natl. Acad. Sci. U. S. A.*, 2014, **111**, 1265–1270.
37 P. C. Mushenheim, R. R. Trivedi, D. B. Weibel and N. L. Abbott, *Biophys. J.*, 2014, **107**, 255–265.
38 S. Zhang, M. A. Greenfield, A. Mata, L. C. Palmer, R. Bitton, J. R. Mantei, C. Aparicio, M. O. de la Cruz and S. I. Stupp, *Nat. Mater.*, 2010, **9**, 594–601.
39 J. B. Matson and S. I. Stupp, *Chem. Commun.*, 2012, **48**, 26–33.
40 S. R. Diegelmann, N. Hartman, N. Markovic and J. D. Tovar, *J. Am. Chem. Soc.*, 2012, **134**, 2028–2031.
41 M. T. McClendon and S. I. Stupp, *Biomaterials*, 2012, **33**, 5713–5722.
42 E. J. Berns, S. Sur, L. Pan, J. E. Goldberger, S. Suresh, S. Zhang, J. A. Kessler and S. I. Stupp, *Biomaterials*, 2014, **35**, 185–195.
43 X. Chen, G. Zhou, X. Peng and J. Yoon, *Chem. Soc. Rev.*, 2012, **41**, 4610–4621.
44 B. E. I. Ramakers, M. van den Heuvel, N. Tsichlis i Spithas, R. P. Brinkhuis, J. C. M. van Hest and D. W. P. M. Löwik, *Langmuir*, 2012, **28**, 2049–2055.
45 B. E. I. Ramakers, S. A. Bode, A. R. Killaars, J. C. M. van Hest and D. W. P. M. Löwik, *J. Mater. Chem. B*, 2015, **3**, 2954–2961.
46 B. D. Wall, S. R. Diegelmann, S. Zhang, T. J. Dawidczyk, W. L. Wilson, H. E. Katz, H.-Q. Mao and J. D. Tovar, *Adv. Mater.*, 2011, **23**, 5009–5014.
47 A. M. Hung and S. I. Stupp, *Nano Lett.*, 2007, **7**, 1165–1171.
48 G. Maret and K. Dransfeld, *Strong and Ultrastrong Magnetic Fields and Their Applications*, Springer, Berlin, Heidelberg, 1985, vol. 57, pp. 143–204.
49 J. Lydon, *J. Mater. Chem.*, 2010, **20**, 10071–10099.
50 V. G. Nazarenko, O. P. Boiko, H. S. Park, O. M. Brodyn, M. M. Omelchenko, L. Tortora, Y. A. Nastishin and O. D. Lavrentovich, *Phys. Rev. Lett.*, 2010, **105**, 017801.
51 T. Ostapenko, Y. A. Nastishin, P. J. Collings, S. N. Sprunt, O. D. Lavrentovich and J. T. Gleeson, *Soft Matter*, 2013, **9**, 9487–9498.
52 We noticed that a part of the **PA** aggregates bundles are not completely aligned parallel or perpendicular to the magnet field direction (Fig. 5c and Fig. 6a, b), which we can attribute to the orthogonal alignment forces acting on the organization of bundled **PA** fibers (positive diamagnetic susceptibility *versus* LCLC template shear and elastic forces) which are in the same order of magnitude. A similar effect was described before in ref. 26.